

**Spin waves in the ferromagnetic metallic manganites  $\text{La}_{1-x}(\text{Ca}_{1-y}\text{Sr}_y)_x\text{MnO}_3$** F. Moussa,<sup>1</sup> M. Hennion,<sup>1</sup> P. Kober-Lehouelleur,<sup>1,\*</sup> D. Reznik,<sup>1,2</sup> S. Petit,<sup>1</sup> H. Moudou, <sup>1</sup> A. Ivanov,<sup>3</sup> Ya. M. Mukovskii,<sup>4</sup> R. Privezentsev,<sup>4</sup> and F. Albenque-Rullier<sup>5</sup><sup>1</sup>Laboratoire Léon Brillouin, CEA-CNRS, CEA Saclay, F-91191 Gif-sur-Yvette Cedex, France<sup>2</sup>Forschungszentrum Karlsruhe, INFP, P. O. Box 3640, D-76021 Karlsruhe, Germany<sup>3</sup>Institut Laue-Langevin, 156 X, 38042 Grenoble Cedex 9, France<sup>4</sup>Moscow State Steel and Alloys Institute, Moscow 119991, Russia<sup>5</sup>Service de Physique de l'Etat Condensé, CEA Saclay, F-91191 Gif-sur-Yvette Cedex, France

(Received 9 February 2007; revised manuscript received 27 April 2007; published 1 August 2007)

We have measured the spin-wave dispersion in the ferromagnetic metallic phase of five manganite compounds:  $\text{La}_{0.7}(\text{Ca}_{1-y}\text{Sr}_y)_{0.3}\text{MnO}_3$  with  $y=0, 0.2, 0.4,$  and  $1$  and  $\text{La}_{0.8}\text{Sr}_{0.2}\text{MnO}_3$ . An apparent broadening of the spin waves at the zone boundary in the  $[001]$  direction was observed, in agreement with previous work. Detailed investigation of this broadening by carefully separating lattice and magnetic contributions to the scattering cross section revealed that this observation is an artifact of the proximity of an optical phonon branch and the magnon branch. Upon separating out the magnon contribution, it becomes clear that the two branches are not strongly coupled and neither mix with nor damp each other within experimental uncertainty. Thus our experiment rules out significant magnon-phonon coupling. We also found that the softening of the spin-wave energy near the zone boundary appears in the manganites with low ( $y=0$ ) and high ( $y=1$ ) Curie temperatures regardless of their crystal structure. Thus it is not related to the existence of correlated polarons. Finally, we report the evolution of the magnetic couplings with doping throughout the whole phase diagram. To explain the observed continuity of the exchange component of the magnetic coupling measured in the metallic phase, we consider a possible persistence of dynamical orbital fluctuations reminiscent of orbital ordering, which occurs in the low-doping insulating regime.

DOI: [10.1103/PhysRevB.76.064403](https://doi.org/10.1103/PhysRevB.76.064403)

PACS number(s): 75.30.Ds, 71.30.+h, 75.30.Et, 75.30.Kz

**I. INTRODUCTION**

The metallic phase of perovskite manganites appears inside a rich and complicated phase diagram in a range of hole doping, beyond a critical value. (See Refs. 1–3 for a general review.) The ferromagnetic metallic phase appears in hole-doped compounds evolving between two end members which have, each one, a peculiar antiferromagnetic insulating ground state. The unusual properties of this metallic phase, and particularly the effect of colossal magnetoresistance (CMR), could be explained by its location in the phase diagram and also by the fundamental properties of the parent compound  $\text{LaMnO}_3$ . In this perovskite, strong electronic correlations compete with electron-lattice interactions, resulting in a long-range-ordered Jahn-Teller distortion combined with a long-range orbital order. Upon hole doping, one creates a system where localized or itinerant charges and spins are strongly coupled to orbital degrees of freedom, giving rise to the spectacular CMR effect. This latter cannot be adequately described by the canonical double-exchange model only.<sup>4,5</sup> We investigated the magnetic metallic phase by measuring its magnetic response function by inelastic neutron scattering. Most published experiments on this topic emphasize a spin-wave dispersion anomaly near the zone boundary, often described as an “anomalous softening” and broadening.<sup>6,7</sup> On the other hand, more conventional spin-wave dispersions have been reported for  $\text{La}_{0.7}\text{Pb}_{0.3}\text{MnO}_3$ .<sup>8</sup> Models have been proposed to account for the spin-wave broadening. Because of the proximity of a longitudinal optic phonon, Furukawa<sup>9</sup> proposes phonon-magnon coupling as the renormalizing mechanism behind the broadening. Khaliullin and Kilian<sup>10</sup>

invoke orbital fluctuations slowed down by a coupling with a particular phonon to explain the zone boundary softening. Recently,<sup>11,12</sup> it has also been shown that the Heisenberg model with an extended range of exchange coupling describes fairly well the anomaly in the measured spin-wave dispersion curves in the metallic phase of a variety of manganites.

Crystal symmetry is another important parameter in these manganites. Depending on the system and on its location in the phase diagram, the structure can be cubic, orthorhombic, or rhombohedral. It is well known that, in the insulating phase, the orthorhombic symmetry is induced by the Jahn-Teller lattice instability and thus favors a tendency to charge ordering.<sup>13,14</sup> This is revealed by neutron and x-ray diffuse scattering observed around the  $(1/4, 1/4, 0)$  reciprocal lattice vector in cubic notation.<sup>15–18</sup> This phenomenon is often described as short-range-correlated lattice polarons. In contrast, no diffuse scattering exists at this point in crystals with a rhombohedral structure. Therefore, in such strongly correlated electron systems, it is natural to ask whether the crystal symmetry plays any role in the softening of the spin waves.

The aim of the present study is to further develop the fundamental understanding of the ferromagnetic metallic phase of perovskite manganites by measuring spin-wave dispersion in  $\text{La}_{1-x}(\text{Ca}_{1-y}\text{Sr}_y)_x\text{MnO}_3$  with  $x=0.3$ . This series has the advantage that all the members have the same doping, making it possible to isolate changes due to structural properties as a function of the average atomic radius of the La, Ca, Sr site, often quoted as the  $A$  site. We have studied four samples with  $y=0, 0.2, 0.4,$  and  $1$ . The first three have an orthorhombic structure and the fourth is rhombohedral. To

complete our survey, we also show the spin-wave dispersion in a Sr-doped compound:  $\text{La}_{0.8}\text{Sr}_{0.2}\text{MnO}_3$ .

We report no measurable magnon-phonon coupling in the ferromagnetic metallic phase, as well as no significant relation between different features of the spin-wave dispersion and the crystal structure. We exclude the idea that the spin-wave dispersion is different for compounds with low and high Curie temperatures. Instead, the characteristics of the spin waves of the metallic phase relate to those of the insulating magnetic phases at lower dopings. We are reminded of the important role played by the trend to an orbital order and to inhomogeneous charge distribution in the low-doping regime. Finally, by reporting the general evolution of the magnetic couplings with doping throughout the phase diagram, we explain the continuity of the exchange coupling values measured in the metallic phase by the possible persistence of dynamical orbital fluctuations as a memory of the orbital order of the lightly doped insulating phases.

This paper is organized as follows. The next section (Sec. II) presents experimental details. Section III presents the results and discusses magnon-phonon coupling. Section IV examines the effect of short-range correlated lattice polarons. Section V focuses on the measurements of  $\text{La}_{0.8}\text{Sr}_{0.2}\text{MnO}_3$ . In Sec. VI, we compare the spin waves in the metallic phase and in the low-doping insulating magnetic phases, we discuss and present concluding remarks on the orbital nature of spin waves in the metallic phase of manganites.

## II. EXPERIMENTAL DETAILS

Single crystals of  $\text{La}_{1-x}(\text{Ca}_{1-y}\text{Sr}_y)_x\text{MnO}_3$  with  $x=0.3$  and  $y=0, 0.2, 0.4$ , and 1, and of  $\text{La}_{1-x}\text{Sr}_x\text{MnO}_3$  with  $x=0.2$  with a volume of about  $0.5 \text{ cm}^3$  and a  $0.6^\circ$  mosaic spread, were grown by the floating zone method in an image furnace. The homogeneity of the doping level in the bulk was carefully checked in all samples. As a result, we had to cut the  $\text{La}_{0.7}\text{Ca}_{0.3}\text{MnO}_3$  single crystal to isolate a homogeneous domain. The homogeneity of the doping rate in the bulk has also been checked by electrical resistivity measurements on thin slices taken at both ends of the sample (see Fig. 1). The magnetic and structural transition temperatures  $T_C$  and  $T_S$  of  $\text{La}_{0.7}(\text{Ca}_{1-y}\text{Sr}_y)_{0.3}\text{MnO}_3$  are summarized in the phase diagram displayed in Fig. 2. The values of  $T_C$  measured in the present work agree with those in the literature.<sup>19,13,14</sup> For  $\text{La}_{1-x}\text{Sr}_x\text{MnO}_3$  with  $x=0.2$ , we have found  $T_C=325 \text{ K}$  and  $T_S=105 \text{ K}$  in agreement with Ref. 20.

Neutron scattering experiments have been performed on triple-axis spectrometers installed at either thermal or cold neutron sources at the reactor ORPHEE of the Laboratoire Léon Brillouin in Saclay and at the Institut Laue-Langevin in Grenoble. These spectrometers are equipped with vertically focusing monochromators and vertically and horizontally focusing analyzers. Energy scans have been performed at a constant scattered neutron wave vector  $k_f$  ( $1.55 \leq k_f \leq 4.1 \text{ \AA}^{-1}$  according to the energy ranges of the study). Each sample was mounted inside an aluminum holder in a double-stage helium closed cryogenerator. The temperature regulation was driven by a digital temperature controller and the stability is better than  $\pm 0.03 \text{ K}$  in the whole temperature range.

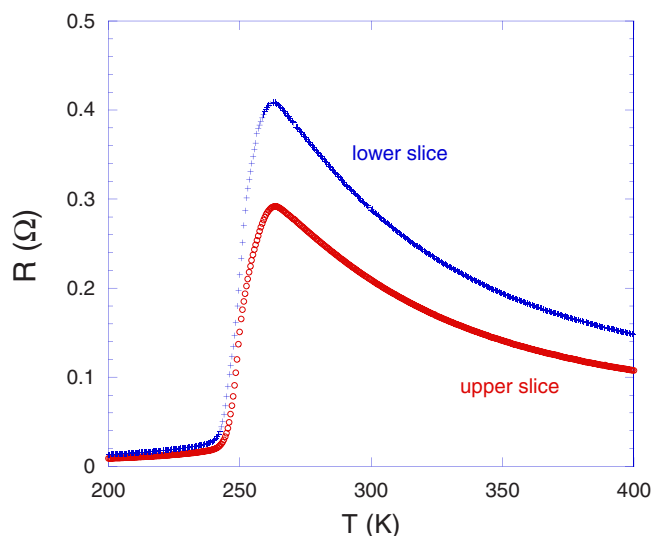


FIG. 1. (Color online) Temperature evolution of the electrical resistance of the upper (red dots) and lower (blue crosses) slices cut in the  $\text{La}_{0.7}\text{Ca}_{0.3}\text{MnO}_3$  single crystal.

All energy spectra (constant  $Q$  scans) were fitted with a sum of several components convoluted with the instrumental resolution function  $R(\mathbf{Q}, \omega)$ . These components were as follows: a  $\delta$  function for the elastic scattering, Lorentzians for the quasielastic and inelastic magnetic scattering, and damped harmonic oscillators for the phonons. The elastic  $q$  scans are described by Lorentzians, whose width is determined by the inverse of the correlation length. The measured intensity at each point of a scan then reads

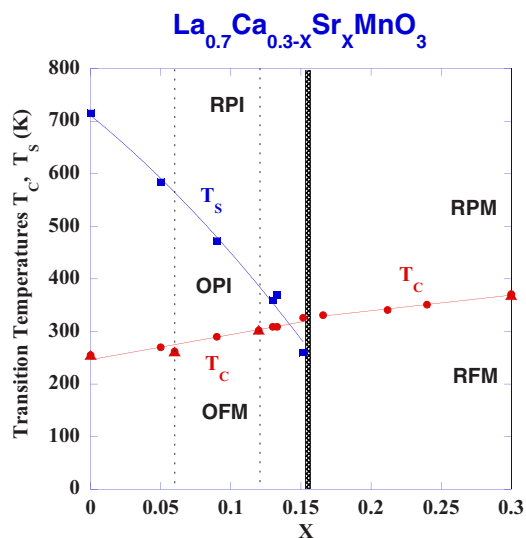


FIG. 2. (Color online) Phase diagram of  $\text{La}_{1-x}(\text{Ca}_{1-y}\text{Sr}_y)_x\text{MnO}_3$  for  $x=0.3$  or  $\text{La}_{0.7}\text{Ca}_{0.3-x}\text{Sr}_x\text{MnO}_3$  with  $X=0.3y$ . Blue squares represent the structural transition temperature  $T_S$  and red dot symbols represent the Curie transition temperature  $T_C$  (Refs. 19, 13, and 14). Red triangles represent our results. RPI, rhombohedral paramagnetic insulating phase; OPI, orthorhombic paramagnetic insulating phase; OFM, orthorhombic ferromagnetic metallic phase; RPM, rhombohedral paramagnetic metallic phase; RFM, rhombohedral ferromagnetic metallic phase.

$$I(\mathbf{Q}_0, \omega_0) = \int R(\mathbf{Q} - \mathbf{Q}_0, \omega - \omega_0) S(\mathbf{Q}, \omega) d^3Q d\omega.$$

The spectral weight  $N(\mathbf{q})$  of the various modes corresponds to their energy integral without the Bose factor. The departure from the cubic structure is very small, and the pseudocubic lattice parameter is nearly the same for all the compounds:  $a \sim 3.87 \text{ \AA}$ . So, to simplify the analysis, we chose the cubic notation and defined  $\mathbf{Q} = \boldsymbol{\tau} + \mathbf{q}$  in cubic indexing. Taking advantage of the form of inelastic neutron scattering cross section,<sup>21</sup> we have measured magnons around  $\boldsymbol{\tau} = (001)$  or  $(110)$  and phonons around  $(002)$  Brillouin zone centers. Unfortunately, phonons contribute to the scattering even around small  $\boldsymbol{\tau}$  values, so we varied the temperature to separate magnetic from phonon scattering.

### III. SPIN WAVES IN $\text{La}_{0.7}(\text{Ca}_{1-y}\text{Sr}_y)_{0.3}\text{MnO}_3$ AND POSSIBLE EFFECT OF MAGNON-PHONON COUPLING

We have measured the spin-wave dispersions in different directions, at several temperatures, for the four samples  $\text{La}_{0.7}(\text{Ca}_{1-y}\text{Sr}_y)_{0.3}\text{MnO}_3$  with  $y=0, 0.2, 0.4, \text{ and } 1$ . Magnon dispersion curves at low temperatures along the  $[001]$  direction, are shown in Fig. 3. For  $y=1$  ( $\text{La}_{0.7}\text{Sr}_{0.3}\text{MnO}_3$ ) our experimental results compare fairly well with the measurements quoted in Ref. 12. This is not exactly the case for  $y=0$ , i.e.,  $\text{La}_{0.7}\text{Ca}_{0.3}\text{MnO}_3$ , where we find higher spin-wave energies near the zone boundary. This discrepancy is perhaps due to a different effective doping rate in the two samples. The double-exchange model developed by Furukawa<sup>22</sup> with two main parameters, the Hund energy  $J_H$  and the electron transfer energy  $t$ , appears to explain the spin-wave dispersion in the low- $q$  range in the metallic phase of Sr-doped compounds<sup>23</sup> and we have tried to apply it to the entire spin-wave dispersion curve of  $\text{La}_{0.7}\text{Ca}_{0.3}\text{MnO}_3$ . Figure 3 shows the best fit with this model using  $J_H = \infty$  and  $t = 0.195 \text{ eV}$ . It is clear that the Furukawa model cannot account for our experimental results. The discrepancy between experiment and theory is the biggest around halfway to the zone boundary, and becomes more and more pronounced with increasing  $y$ . A Heisenberg model with only the first-neighbor interaction is not suitable either. If the fitting parameter is chosen here to describe the spin-wave dispersion in the low- $q$  region, then the measured high- $q$  spin-wave energies are systematically smaller than the calculated ones. This is commonly referred to as the softening or the anomaly of the spin-wave dispersion curve near the zone boundary. In contrast, the whole experimental data set is better described with a spin-wave dispersion law  $\omega(\zeta) = 4SJ_1[1 - \cos(2\pi\zeta)] + 4SJ_4[1 - \cos(4\pi\zeta)]$ , derived from a Heisenberg Hamiltonian where  $J_1$  and  $J_4$  are the first- and fourth-neighbor couplings as in Refs. 11 and 12. The results of the fit within this model are represented by the solid and dashed lines in Fig. 3 together with  $J_1$  and  $J_4$  plotted as a function of  $y$ .  $J_1$  remains nearly constant, while  $J_4$  increases by a factor of 2, from  $y=0$  to 1.

This zone boundary softening can also be reproduced theoretically by a regular assembly of spins with first-neighbor coupling  $J_1$ , with a random spatial distribution of a

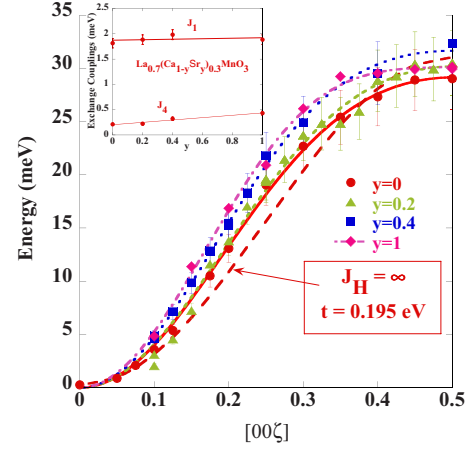


FIG. 3. (Color online) Spin-wave dispersion curves at low temperature in the  $[00\zeta]$  direction of  $\text{La}_{0.7}(\text{Ca}_{1-y}\text{Sr}_y)_{0.3}\text{MnO}_3$ .  $y=0$ ,  $T=13.4 \text{ K}$ , red dots;  $y=0.2$ ,  $T=30 \text{ K}$ , green triangles;  $y=0.4$ ,  $T=23 \text{ K}$ , blue squares;  $y=1$ ,  $T=31 \text{ K}$ , pink diamonds. The thick broken red line represents the best fit to the model of Ref. 22 for the  $y=0$  sample. The other lines represent the best fit to  $\omega(\zeta) = 4SJ_1[1 - \cos(2\pi\zeta)] + 4SJ_4[1 - \cos(4\pi\zeta)]$  as in Refs. 11 and 12: red solid line for  $y=0$ ; green dashed line for  $y=0.2$ ; blue dotted line for  $y=0.4$ ; pink dash-dotted line for  $y=1$ . Inset: Evolution with  $y$  of first- and fourth-neighbor couplings  $J_1$  and  $J_4$ .

different first-neighbor coupling  $J'_1$  acting as defects in the mean magnetic structure.<sup>24</sup>

Now, we examine whether the magnon-phonon coupling could explain the experimental spin-wave broadening near the zone boundary. Let us consider, as an example, the case of  $\text{La}_{0.7}\text{Ca}_{0.3}\text{MnO}_3$ . Figure 4 shows the experimental phonon as well as the spin-wave dispersions.

As the LO1 branch crosses the spin-wave curve, a magnon-phonon coupling is *a priori* possible, as described in Ref. 9. In addition, phonons of large wave number are measurable even in the  $(001)$  Brillouin zone. At first glance, the spectrum taken at low temperature near the zone boundary may appear broad, as if the magnon is damped by phonons (Fig. 5). But by performing a precise temperature study of the magnon at  $\mathbf{q}=(0,0,0.45)$ , we established that the line shape of the magnon spectrum at  $T=13 \text{ K}$  is broadened by the presence side by side of noninteracting magnons and phonons if the phonon intensity is erroneously assigned to magnetic scattering. At room temperature, the spin excitation peak ( $Mg$  in Fig. 5), is quasielastic, and the remaining inelastic scattering is due to the longitudinal acoustic (LA) and optic (LO1) phonons ( $Ph$  in Fig. 5). Their characteristics [energy  $\omega_{\mathbf{q}}$ , width  $\Gamma(\mathbf{q})$ , spectral weight  $N(\mathbf{q})$ ] are determined at this temperature. In the fitting procedure for all the low-temperature spectra we made the simplest assumption, i.e., that the phonons are temperature independent (Fig. 5). As the temperature increases, one clearly sees in Fig. 5 a classical renormalization of the spin-wave mode toward zero energy at  $T=T_C$ . Furthermore, there is no enhanced damping of the spin waves at the low temperatures in the entire Brillouin zone, as shown in the upper panel of Fig. 4, where the damping constant  $\Gamma$  is plotted versus the spin-wave energy  $\omega$ . The ratio  $\Gamma/\omega$  is less than  $1/8$  in the whole Brillouin zone.

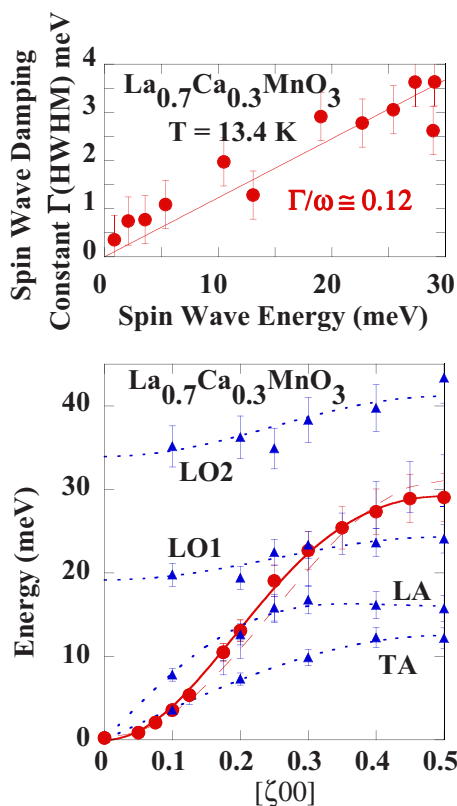


FIG. 4. (Color online) Spin-wave (red dots) and phonon (blue triangles) dispersion curves in  $\text{La}_{0.7}\text{Ca}_{0.3}\text{MnO}_3$ . Magnons were measured around (001) at  $T=13.4$  K and phonons were measured around (002) and (020) at  $T=295$  K. Dotted lines are a guide for the eye for the phonons. The broken and solid lines are the same as in Fig. 3. The upper panel shows the spin wave damping constant  $\Gamma$  [half width at half maximum (HWHM)] versus the spin-wave energy in  $\text{La}_{0.7}\text{Ca}_{0.3}\text{MnO}_3$  at  $T=13.4$  K. The different values of  $\Gamma$  are comparable to the energy resolution of the spectrometer in this energy range.

The low-energy phonon dispersions have been determined around large  $\tau$  values in all investigated compounds. They compare well with those of  $\text{La}_{0.7}\text{Sr}_{0.3}\text{MnO}_3$ , measured by Reichardt and Braden.<sup>25</sup> Isolating the phonon by measuring at large wave vectors as opposed to raising the temperature produces the same results, i.e., the magnons do not appear strongly damped. So we conclude that the apparent broadening of the spin waves when they cross a phonon branch is due to the overlap of magnon and phonon dispersion curves, and is not the result of magnon-phonon coupling. The same conclusion has been drawn from a polarized neutron scattering experiment on a sample of  $\text{La}_{0.7}\text{Ca}_{0.3}\text{MnO}_3$ .<sup>26</sup>

The same study has been also carried out along the [110] direction for three compounds with  $y=0, 0.2, \text{ and } 1$ . The results are reported in Fig. 6. In that direction too, phonons could be detected even around small  $\tau$  values, as was the case for  $\mathbf{q}=(0.2, 0.2, 1)$ , especially the LA phonon. The same analysis of the experimental data led us to the same conclusion as for the [001] direction.

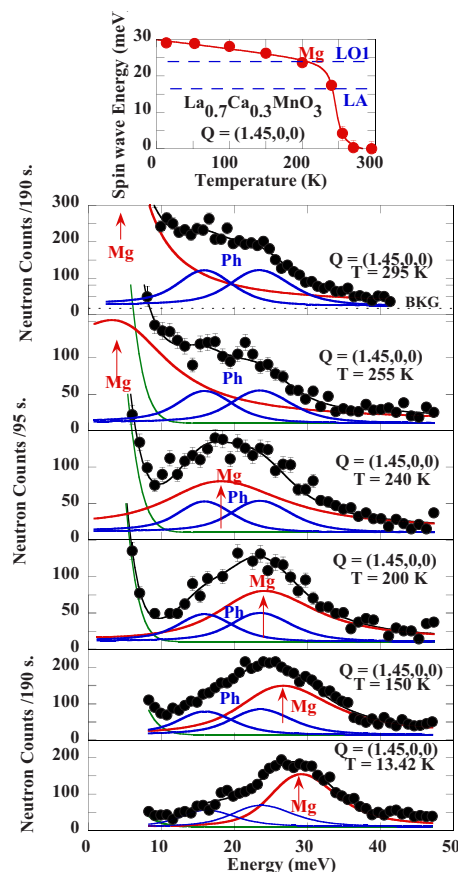


FIG. 5. (Color online) Example of energy spectra at  $\mathbf{Q}=(1.45, 0, 0)$  at different temperatures. Phonons (Ph, blue lines) and magnon (Mg, red line) modes are respectively fitted with damped harmonic oscillators and with Lorentzians. Phonon fitting parameters were fixed as described in the text. Top panel: Temperature evolution of the magnon energy (the red solid line and the blue dashed lines are guides for the eye). LA, longitudinal acoustic phonon; LO1, lowest-energy longitudinal optic phonon.

#### IV. SPIN WAVES AND SHORT-RANGE-CORRELATED LATTICE POLARONS

It is well known that the manganites which have an insulating, orthorhombic paramagnetic phase have short-range-correlated lattice polarons. They result from a strong electron-lattice interaction, which induces lattice distortions,<sup>13,14</sup> and the subsequent tendency to charge ordering. This leads to long-range order which transforms at lower temperature into a peculiar antiferromagnetic order, known as CE order at  $x=0.5$ , as in  $\text{Pr}_{0.5}\text{Ca}_{0.5}\text{MnO}_3$ .<sup>1</sup> These correlated lattice defects have been revealed by neutron and x-ray diffuse scattering at  $\mathbf{Q}=\tau+\mathbf{q}$  with large  $\tau$  and with  $\mathbf{q}=(0.25, 0.25, 0)$ .<sup>15–18</sup>

As this diffuse scattering is measurable only around large  $\tau$ , this means that it comes only from the lattice. This has been confirmed by polarized neutron measurements in  $\text{La}_{0.7}\text{Ca}_{0.3}\text{MnO}_3$ .<sup>27</sup> We have studied diffuse scattering induced by the short-range correlated polarons, in four systems: three orthorhombic compounds  $\text{La}_{0.7}(\text{Ca}_{1-y}\text{Sr}_y)_{0.3}\text{MnO}_3$  with  $y=0, 0.2, \text{ and } 0.4$  and the rhombohedral one with  $y=1$  ( $\text{La}_{0.7}\text{Sr}_{0.3}\text{MnO}_3$ ). As expected,<sup>17,18</sup>

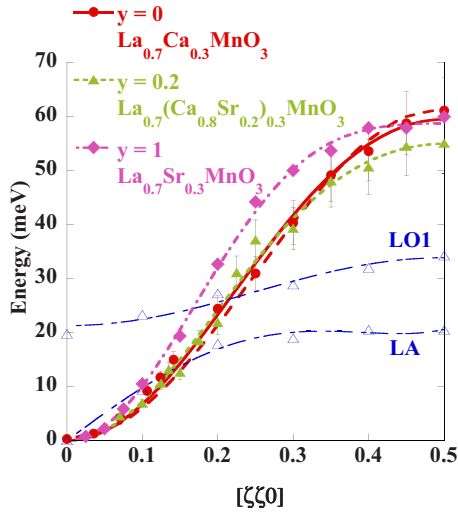


FIG. 6. (Color online) Spin-wave dispersion curves at low temperature in the  $[\zeta, \zeta, 0]$  direction of  $\text{La}_{0.7}(\text{Ca}_{1-y}\text{Sr}_y)_{0.3}\text{MnO}_3$ .  $y=0$ , red dots;  $y=0.2$ , green triangles;  $y=1$ , pink diamonds. The lines have the same meaning as in Fig. 3. Blue empty triangles represent phonons and the lines through them are guides for the eye.

we observed that there is no diffuse scattering around  $\mathbf{q} = (0.25, 0.25, 0)$  in the  $\text{La}_{0.7}\text{Sr}_{0.3}\text{MnO}_3$  sample.

Two  $q$  scans, at 270 and at 624 K, are shown in Fig. 7 for  $\text{La}_{0.7}\text{Ca}_{0.3}\text{MnO}_3$ . They show that the intensity of the modulation reaches its maximum around  $T_C$ , and decreases above. At 624 K, in spite of the small intensity, the modulation is still observed although it is broader. The upper panel of Fig. 7 displays the temperature evolution of the correlation length  $\xi$  where a pronounced maximum appears around  $T_C$ .

Very similar spectra are observed in the mixed compounds  $\text{La}_{0.7}(\text{Ca}_{1-y}\text{Sr}_y)_{0.3}\text{MnO}_3$ , but with some differences: the modulation becomes less pronounced and broader when  $y$  increases from 0 to 0.4.

The temperature evolution of the diffuse intensity measured at the point  $\mathbf{q} = (0.25, 0.25, 0)$  is displayed in Fig. 8 for the three compounds. In  $\text{La}_{0.7}\text{Ca}_{0.3}\text{MnO}_3$ , it decreases abruptly below  $T_C$ , in the metallic phase. In the compounds with  $y=0.2$  and 0.4, the maximum intensity is smaller and the decrease below  $T_C$  is also smaller. This means that the first-order character of the insulator-metal transition at  $T_C$  is less pronounced in the mixed compounds than in the pure Ca-doped compound. We also observed that far from  $T_C$  the diffuse intensity vanishes very fast in the  $y=0.4$  compound. For temperatures much larger than  $T_C$ , this can be explained by the closeness of the orthorhombic-rhombohedral structural transition temperature  $T_S$  which is much lower in this compound than in the two others. We have also extensively studied the dynamics of these correlated polarons. Figure 9 shows a room temperature energy spectrum of  $\text{La}_{0.7}\text{Ca}_{0.3}\text{MnO}_3$ . It has an elastic component, and a quasi-elastic one. The latter has a width  $\Gamma = 2.3$  meV, which is much larger than the experimental resolution (0.6 meV). The same figure also shows the temperature evolution of the main characteristics of this spectrum. The width of the quasielastic component,  $\Gamma$ , does not vary significantly, whereas its intensity  $N_{quasi}$  as well as the intensity of the elastic peak,  $N_{el}$ ,

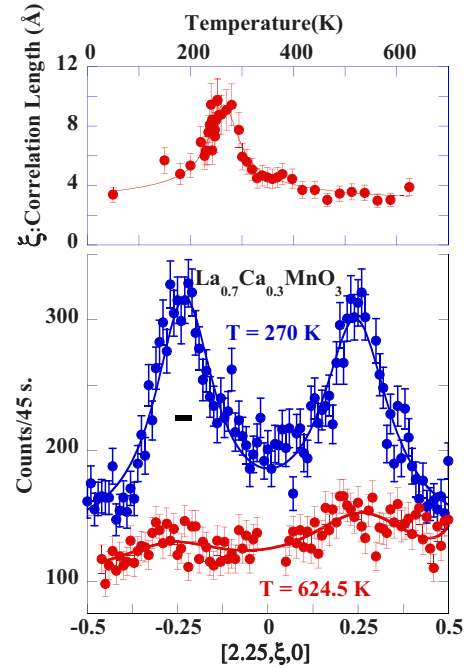


FIG. 7. (Color online) Correlated polarons in  $\text{La}_{0.7}\text{Ca}_{0.3}\text{MnO}_3$  ( $T_C=255$  K). Lower panel: Two selected elastic scans along  $[2.25, \xi, 0]$  showing a maximum diffuse scattering at  $\xi = \pm 0.25$  at  $T=270$  (blue symbols) and 624.5 K (red symbols). Lines are the results of a fit with Lorentzians. The thick black bar (not on scale) is the elastic  $q$  resolution of the spectrometer: full width at half maximum  $\Delta Q = 0.02$  in r.l.u. Upper panel: Temperature evolution of the correlation length  $\xi$  in  $\text{\AA}$  (inverse of the width) of correlated polarons. Note the maximum around  $T_C$ . The line is a guide for the eye.

decrease slowly and monotonically with increasing temperature above  $T_C$ . There is no indication of any freezing or slowing down of these dynamics at a particular temperature  $T^*$  as observed in the bilayer manganite.<sup>28</sup> In that case, it is possible that the two-dimensional character favors such a freezing, while the nearly cubic symmetry of the present compounds does not.

It is now well established that the maximum colossal magnetoresistance effect occurs in systems with correlated lattice polarons in their paramagnetic phase. They play the role of a charge reservoir. In contrast, in compounds such as  $\text{La}_{0.7}\text{Sr}_{0.3}\text{MnO}_3$  where no correlated lattice polarons are detected, the CMR effect appears to be rather conventional.<sup>13</sup>

In the four presently studied compounds, the spin-wave dispersion curves have similar features regardless of their structure. The three orthorhombic compounds with lattice polarons as well as the rhombohedral compound without such polarons display a zone boundary softening of spin waves. So the lattice polarons, which are obviously essential to explain the CMR, do not seem to be very involved in the spin dynamics of the metallic phase. However, the value of  $J_4$ , the exchange coupling between fourth Mn neighbours, which are two lattice parameters apart, increases by a factor of 2 from the compound  $\text{La}_{0.7}\text{Ca}_{0.3}\text{MnO}_3$  ( $y=0$ ) to the compound  $\text{La}_{0.7}\text{Sr}_{0.3}\text{MnO}_3$  ( $y=1$ ) (see the inset in Fig. 3). This feature could be explained by the continuous increase of the

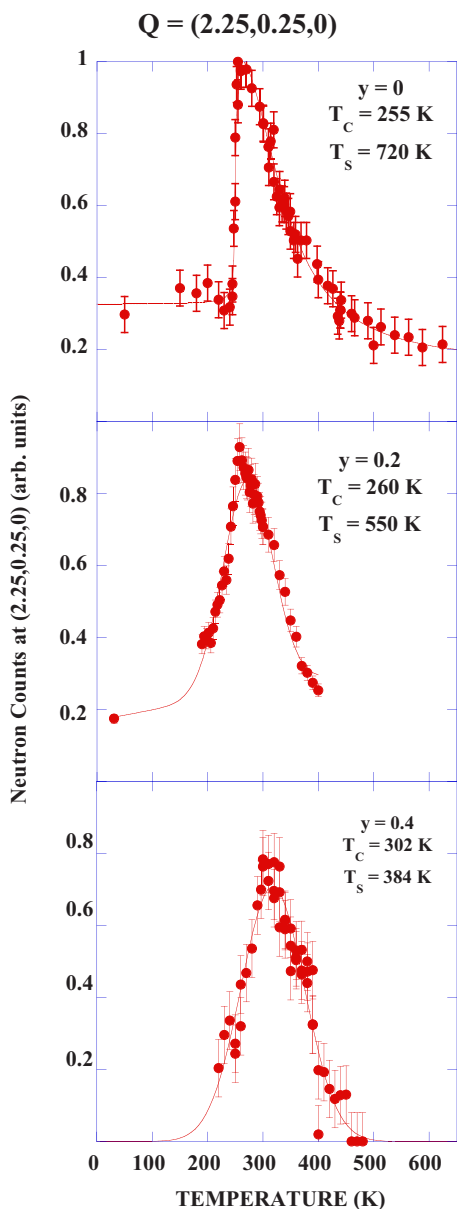


FIG. 8. (Color online) Comparison of the temperature evolution of the diffuse scattering intensity at  $\mathbf{Q}=(2.25, 0.25, 0)$  for three compounds  $\text{La}_{0.7}(\text{Ca}_{1-y}\text{Sr}_y)_{0.3}\text{MnO}_3$ : from top to bottom,  $y=0, 0.2,$  and  $0.4$ . Solid lines are guides for the eye.

average radius of the A-site cation in the  $0 \leq y \leq 1$  range, leading to fewer and fewer distorted  $\text{MnO}_6$  octahedra, and thus to a decreased bending of Mn-O-Mn bonds. This, in turn, results in an increase of the electronic bandwidth. So, from  $\text{La}_{0.7}\text{Ca}_{0.3}\text{MnO}_3$  to  $\text{La}_{0.7}\text{Sr}_{0.3}\text{MnO}_3$ , the metallicity improves and the exchange coupling at a larger distance increases.

V. SPIN WAVES IN  $\text{La}_{0.8}\text{Sr}_{0.2}\text{MnO}_3$  COMPOUND

We also report the results of spin-wave measurements in  $\text{La}_{0.8}\text{Sr}_{0.2}\text{MnO}_3$  ( $T_C=325$  K). Figure 10 shows dispersion curves along the [001] and [111] directions. They are well fitted by a first-neighbor Heisenberg model with one ex-

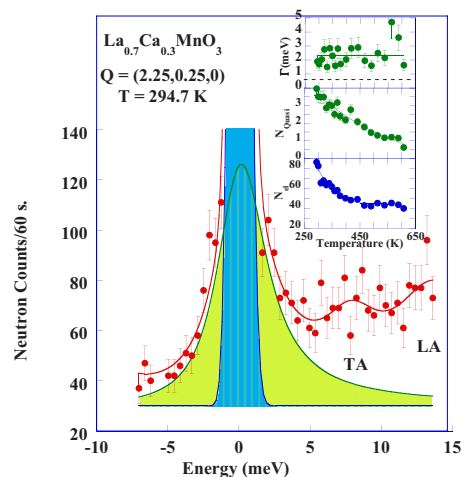


FIG. 9. (Color online) Energy scan in  $\text{La}_{0.7}\text{Ca}_{0.3}\text{MnO}_3$  at  $\mathbf{Q}=(2.25, 0.25, 0)$  and  $T=294.7$  K. The spectrum is analyzed with two main components centered at zero energy: an elastic one ( $\delta$  function, narrow blue line) and a quasielastic one (Lorentzian, broader green line). Two inelastic modes are also seen (TA and LA). Inset: Temperature evolution of, from top to bottom, the quasielastic width  $\Gamma$  (meV), (black dashed line indicates the incoherent energy resolution (HWHM) of the spectrometer), the quasielastic component  $N_{quasi}$  (green symbols), and the elastic component  $N_{el}$  (blue symbols). Lines are guides for the eye.

change coupling:  $J=2.3$  meV. The fit is not significantly improved with fourth-neighbor extended ferromagnetic coupling  $J_4$  as in the model developed in Refs. 11 and 12. We find a very small value,  $J_4=0.09$  meV, just within the experimental uncertainty. Interestingly, Ye *et al.*<sup>12</sup> have found the same spin-wave behavior ( $J_4 \sim 0$ ) in  $\text{La}_{0.75}\text{Ca}_{0.25}\text{MnO}_3$  ( $T_C=191$  K). So, independent of the system, on entering the metallic phase, the spin-wave dispersion does not exhibit a flattening near the zone boundary, i.e., it is well represented by the first-neighbor coupling  $J_1$ . With increased doping, a softening of the spin-wave energy around the zone boundary appears equally in the Sr-doped and Ca-doped compounds.

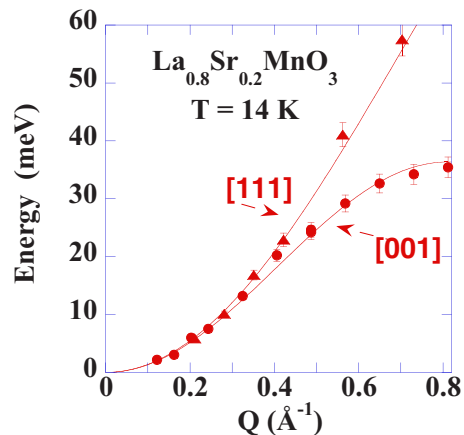


FIG. 10. (Color online) Spin-wave dispersion curves along [001] (red dots) and [111] (red triangles) at  $T=14$  K in  $\text{La}_{0.8}\text{Sr}_{0.2}\text{MnO}_3$ . Solid lines show the best fit with  $J_1=2.3$  meV and  $J_4=0$ .

The similarity of the spin-wave dispersions of the four samples with  $x=0.3$  [ $\text{La}_{0.7}(\text{Ca}_{1-y}\text{Sr}_y)_{0.3}\text{MnO}_3$  with  $y=0, 0.2, 0.4,$  and  $1$ ] and the two compounds  $\text{La}_{0.8}\text{Sr}_{0.2}\text{MnO}_3$  and  $\text{La}_{0.75}\text{Ca}_{0.25}\text{MnO}_3$  rules out the generally accepted idea that high Curie temperature perovskites (e.g.,  $\text{La}_{0.7}\text{Sr}_{0.3}\text{MnO}_3$ ,  $T_C=370$  K) and low Curie temperature perovskites (e.g.,  $\text{La}_{0.7}\text{Ca}_{0.3}\text{MnO}_3$ ,  $T_C=255$  K) have different spin-wave dispersions (Ref. 3, p. 225 or Ref. 10). The following section addresses the origin of the magnetic couplings.

## VI. DISCUSSION AND CONCLUDING REMARKS ON THE FERROMAGNETIC METALLIC PHASE

To better understand the observed behavior of spin waves in the metallic phase, we consider a possible continuity of the magnetic coupling throughout the whole phase diagram. We focus on both series of compounds, Sr-doped and Ca-doped systems, but not on the mixed compounds. We include in the metallic part of their phase diagram the results of the present study on  $x_{\text{Ca}}=0.3$ ,  $x_{\text{Sr}}=0.2$ , and  $x_{\text{Sr}}=0.3$ ; the results on the latter agree with those reported in Ref. 12. We include also not yet published results,<sup>24</sup> on  $x_{\text{Ca}}=0.22$  and on  $x_{\text{Sr}}=0.17$ .

In  $\text{La}_{1-x}\text{Ca}_x\text{MnO}_3$  and  $\text{La}_{1-x}\text{Sr}_x\text{MnO}_3$ , in the low-doping regime  $0 \leq x < x_c$  ( $x_c=0.225$  and  $0.175$ , respectively),<sup>29-40</sup> features of the spin-wave spectrum allowed us to define two types of coupling, which have been related to hole-rich or hole-poor regions.

The hole-rich type of coupling, rather associated with double exchange, is provided by the dispersion curve defined in the small- $q$  range only, which appears with doping. A spin-wave stiffness constant  $D$  can be derived from the parabolic form  $\hbar\omega=Dq^2$ .<sup>41</sup>

The hole-poor type of coupling can be extracted from the higher energy part of the spin wave spectrum. It consists either of a continuous spin wave curve with a large gap in the canted antiferromagnetic (CAF) state ( $x < 0.125$ ) where the hole-poor region is large and percolative,<sup>30-32,34,36</sup> or of distinct energy levels, when it is reduced to small domains ( $0.125 < x < x_c$ ).<sup>33,35,39,40</sup> In both cases, the ‘‘hole-poor’’ character with the same kind of orbital order as in the parent compound  $\text{LaMnO}_3$ ,<sup>29,42</sup> was deduced from the fact that the spin-wave spectrum was well described by a Heisenberg model with *anisotropic* first-neighbor exchange couplings:  $J_{a,b}$  coupling the Mn ions in the basal (**a**, **b**) plane and  $J_c$  coupling the Mn ions along the **c** axis (as in  $\text{LaMnO}_3$ ).

In the metallic phase, where  $x > x_c$ , the three directions associated with the three nearly cubic edges **a**, **b**, and **c** become equivalent. The spin-wave spectrum reorganizes into an isotropic universal dispersion curve characterized by spin-wave stiffness  $D$  determined by the parabolic law  $\hbar\omega=Dq^2$  in the low- $q$  range. The first-neighbor exchange coupling also becomes isotropic:  $J_{a,b}=J_c=J_1$ . It is mainly determined by the energy of the spin-wave modes measured at the zone boundaries in different directions. We have plotted the values of  $D$ ,  $J_{a,b}$ , and  $J_c$ , then  $J_1$ , versus  $x$  for both systems, in Fig. 11. We have also put on the same plot, results on the same compounds, taken from the literature. Both series have many similarities but have different values of  $D$ . While there is a

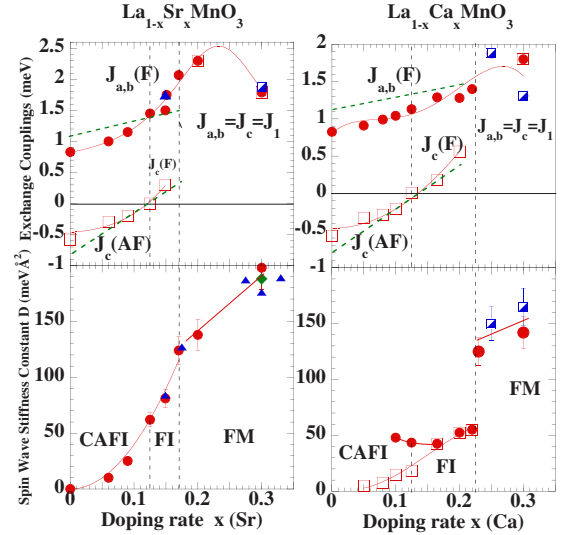


FIG. 11. (Color online) Evolution of magnetic couplings with the doping rate, in Sr-doped (left panels) and Ca-doped (right panels) systems. Red full dots and red empty squares represents our previous and present results. We add also not yet published results on two compounds, one with  $x_{\text{Sr}}=0.17$  and one with  $x_{\text{Ca}}=0.22$  (Ref. 24). Blue triangles represent the data from Refs. 23, 46, and 47. Half full blue squares represent the data from Ref. 12 and from works quoted in it. Green diamond represents data from Ref. 48. Red lines are guides for the eye. CAFI, canted antiferromagnetic insulating phase; FI, ferromagnetic insulating phase; FM, ferromagnetic metallic phase. Upper panels: First-neighbor exchange coupling.  $0 \leq x < x_c$ , anisotropic coupling:  $J_{a,b}$ , red full dots and  $J_c$ , red empty squares.  $x_c \leq x$ , isotropic coupling:  $J_{a,b}=J_c=J_1$ . Green dotted lines represent calculated exchange couplings from Ref. 43. Lower panels: Spin-wave stiffness constant  $D$ . Red full dots represent  $D$  in plane and red empty squares  $D$  along **c**.  $D$  becomes isotropic much before  $x_c$ . At  $x=x_c$ , note the continuity of  $D$  in the Sr-doped compounds and the jump in the Ca-doped compounds.

pronounced jump of  $D$  for the Ca system at the insulator-metal transition, the jump is small or nearly zero (within the experimental accuracy) for the Sr one. In the metallic phase, in the Ca system,  $D$  can be considered as either slowly increasing with the doping rate  $x$ , or nearly constant, in agreement with the results of Ref. 12. In the Sr system,  $D$  increases continuously in agreement with the improvement of the metallicity. We also observe that, for both systems,  $J_{a,b}$  and then  $J_1$  in the metallic phase evolve continuously throughout the doping range  $0 \leq x \leq 0.3$ , going through a maximum around  $x=0.25$  and decreasing beyond. The continuity is less evident for  $J_c$ , and it could have a discontinuity at  $x=x_c$ . How to interpret these results?

To explain the jump of  $D$ , in Ca-doped system, at the insulator-metal transition occurring at  $x=x_c$ , we invoke the role of correlated lattice polarons present in the insulating phase of this system. Their size is large enough to prevent strong magnetic coupling detected in long-wavelength spin waves. When the correlated polarons disappear, at  $x=x_c$ , in the metallic phase, then  $D$  reaches nearly the same value as in the Sr-doped system in agreement with the results of Ref. 12.

The increase with doping of  $J_{a,b}$  and  $J_c$  in the low-doping insulating phases is nearly quantitatively reproduced by the

theory developed by Feiner and Oleś<sup>43</sup> from the long-range orbital order stabilized by the Jahn-Teller effect and renormalized by the double-exchange coupling (see the dotted green lines in Fig. 11). So, the monotonic evolution of  $J_{a,b}$  and then  $J_1$  in the metallic phase through the insulator-metal transition leads to the conclusion that the same type of orbital order is involved when the systems enter the metallic phase. This suggestion is different from what is expected in a metallic magnetic phase, where, theoretically, the  $e_g$  orbitals ( $3z^2-r^2$  and  $x^2-y^2$ ) are degenerate and the electronic state is described by an orbital liquid (i.e., orbital-disordered) state.<sup>44</sup> However, we think that the strong tendency to orbital ordering fully developed in the parent compound  $\text{LaMnO}_3$  and in the insulating phases at low doping, is manifested as fluctuations.

We suggest also that this short-range orbital order is compatible with the decrease of the first-neighbor magnetic coupling  $J_1=J_{ab}=J_c$  when  $x_{\text{Sr}}$  goes from 0.2 to 0.3 or when  $x_{\text{Ca}}$  varies from 0.25 to 0.3 (Fig. 11). In both Ca-doped and Sr-doped systems, there is a tendency for  $J_1$  to be maximum around  $x=0.25$ . If we describe the spin-wave dispersion curve in the metallic phase by the Heisenberg model with two exchange couplings  $J_1$  (between first neighbors) and  $J_4$  (between fourth neighbors) as in Refs. 11 and 12, we observe that this decrease of  $J_1$  is accompanied by the appearance of  $J_4$ . So, in these systems, the improvement of metallicity is revealed by an extension of the range of the magnetic coupling at the expense of the first-neighbor interaction. This conclusion differs from that of Endoh *et al.*,<sup>11</sup> who indicate that  $J_1$  may rather be related to  $(x^2-y^2)$ -type orbital when  $J_4=0$ , while  $(3z^2-r^2)$ -type orbital correlations may explain the relatively high value found for  $J_4$  in  $\text{Sm}_{0.55}\text{Sr}_{0.45}\text{MnO}_3$ . We suggest that the change toward  $(x^2-y^2)$ -type orbitals would rather occur in more exotic states, like the metallic antiferromagnetic state at larger doping of the Sr-doped system.<sup>45</sup> Actually, many competing interactions have to be taken into account to explain the behavior of spin dynamics, as is concluded in Ref. 12. Our suggestion of short-range  $(3z^2-r^2)$ -type orbital fluctuations emphasizes just one of the important ones.

The outstanding role of the orbitals in the metallic state mentioned here has often been invoked in theoretical works (see, for instance, Ref. 10 and references therein<sup>10</sup>).

In summary, we have measured spin-wave dispersions in the ferromagnetic metallic phase of five manganite compounds.

We have explored mixed compounds at the same doping level  $x=0.3$ . This chemical series connects two different series of manganites: the Ca-doped ones, with low  $T_C$ , large CMR effect, and orthorhombic structure allowing correlated lattice polarons in its paramagnetic phase, and the Sr-doped ones, with high  $T_C$ , conventional CMR effect, and rhombohedral structure without correlated polarons.

First, we have shown that the apparent broadening of spin waves was due to an overlap with an independent phonon branch. Once the phonon and magnon contributions to the measured neutron scattering intensities were taken into account, magnons appeared not to be strongly damped, and so we have excluded the possibility of magnon-phonon coupling.

Second, we have shown that the spin-wave dispersion curves of the four compounds  $\text{La}_{0.7}(\text{Ca}_{1-y}\text{Sr}_y)_{0.3}\text{MnO}_3$  exhibited the same kind of softening near the zone boundary. This feature was well described by a Heisenberg model with two exchange couplings  $J_1$  and  $J_4$ . We have observed that  $J_4$  increases regularly with  $y$  and changes by a factor of 2 from  $y=0$  to 1. We have related this behavior to the concomitant increase of the average radius of the  $A$ -site cation. This effect enhances the electronic bandwidth and strengthens the magnetic coupling at larger distance.

The study of  $\text{La}_{0.8}\text{Sr}_{0.2}\text{MnO}_3$  has allowed us to enrich the metallic and ferromagnetic part of the phase diagram of Sr-doped compounds and revealed great similarities between the Ca-doped and Sr-doped chemical series.

Finally, by reporting the general evolution with doping of the magnetic couplings through the whole phase diagram, we propose to explain the continuity of the exchange coupling values measured in the metallic phase by dynamical orbital fluctuations reminiscent of orbital order in the insulating phases, which still persist in the metallic phase.

#### ACKNOWLEDGMENTS

Two authors (F.M. and M.H.) are very grateful to J. A. Fernandez-Baca for communicating data on Ca-doped compounds before publication and for stimulating discussions. We further acknowledge A. M. Oleś and M. B. Lepetit for fruitful exchanges.

\*Present address: ICCN, NXP, Philips, 2 rue de la Girafe, F-14059 Caen, Cedex 5, France.

<sup>1</sup> *Colossal Magnetoresistance of Manganese Oxides*, edited by C. N. R. Rao and B. Raveau (World Scientific, Singapore, 1998).

<sup>2</sup> *Colossal Magnetoresistive Oxides*, edited by Y. Tokura (Gordon and Breach Science Publishers, New York, 2000).

<sup>3</sup> E. Dagotto, *Nanoscale Phase Separation and Colossal Magnetoresistance*, Springer Series in Solid-State Sciences Vol. 136 (Springer-Verlag, Berlin, 2003).

<sup>4</sup> C. Zener, *Phys. Rev.* **82**, 403 (1951).

<sup>5</sup> P. G. de Gennes, *Phys. Rev.* **118**, 141 (1960).

<sup>6</sup> H. Y. Hwang, P. Dai, S-W. Cheong, G. Aeppli, D. A. Tennant, and H. A. Mook, *Phys. Rev. Lett.* **80**, 1316 (1998).

<sup>7</sup> P. Dai, H. Y. Hwang, Jiandi Zhang, J. A. Fernandez-Baca, S-W. Cheong, C. Kloc, Y. Tomioka, and Y. Tokura, *Phys. Rev. B* **61**, 9553 (2000).

<sup>8</sup> T. G. Perring, G. Aeppli, S. M. Hayden, S. A. Carter, J. P. Re-meika, and S-W. Cheong, *Phys. Rev. Lett.* **77**, 711 (1996).

<sup>9</sup> N. Furukawa, *J. Phys. Soc. Jpn.* **68**, 2522 (1999).

<sup>10</sup> G. Khaliullin and R. Kilian, *Phys. Rev. B* **61**, 3494 (2000).

<sup>11</sup> Y. Endoh, H. Hiraka, Y. Tomioka, Y. Tokura, N. Nagaosa, and T. Fujiwara, *Phys. Rev. Lett.* **94**, 017206 (2005).

- <sup>12</sup>F. Ye, Pengcheng Dai, J. A. Fernandez-Baca, Hao Sha, J. W. Lynn, H. Kawano-Furukawa, Y. Tomioka, Y. Tokura, and Jiandi Zhang, *Phys. Rev. Lett.* **96**, 047204 (2006).
- <sup>13</sup>Y. Tomioka, A. Asamitsu, and Y. Tokura, *Phys. Rev. B* **63**, 024421 (2001).
- <sup>14</sup>J. Mira, J. Rivas, L. E. Hueso, F. Rivadulla, M. A. López Quintela, M. A. Señarís Rodríguez, and C. A. Ramos, *Phys. Rev. B* **65**, 024418 (2002).
- <sup>15</sup>Pengcheng Dai, J. A. Fernandez-Baca, N. Wakabayashi, E. W. Plummer, Y. Tomioka, and Y. Tokura, *Phys. Rev. Lett.* **85**, 2553 (2000).
- <sup>16</sup>C. P. Adams, J. W. Lynn, Y. M. Mukovskii, A. A. Arsenov, and D. A. Shulyatev, *Phys. Rev. Lett.* **85**, 3954 (2000).
- <sup>17</sup>V. Kiryukhin, T. Y. Koo, H. Ishibashi, J. P. Hill, and S-W. Cheong, *Phys. Rev. B* **67**, 064421 (2003).
- <sup>18</sup>V. Kiryukhin, A. Borissov, J. S. Ahn, Q. Huang, J. W. Lynn, and S-W. Cheong, *Phys. Rev. B* **70**, 214424 (2004).
- <sup>19</sup>P. G. Radaelli, M. Marezio, H. Y. Hwang, S-W. Cheong, and B. Batlogg, *Phys. Rev. B* **54**, 8992 (1996).
- <sup>20</sup>H. Kawano, R. Kajimoto, M. Kubota, and H. Yoshizawa, *Phys. Rev. B* **53**, R14709 (1996).
- <sup>21</sup>S. W. Lovesey, *Theory of Neutron Scattering from Condensed Matter* (Clarendon Press, Oxford, 1987).
- <sup>22</sup>N. Furukawa, *J. Phys. Soc. Jpn.* **65**, 1174 (1996).
- <sup>23</sup>A. H. Moudden, L. Vasiliu-Doloc, L. Pinsard, and A. Revcolevschi, *Physica B* **241–243**, 276–280 (1998).
- <sup>24</sup>S. Petit (unpublished).
- <sup>25</sup>W. Reichardt and M. Braden, *Physica B* **263–264**, 416 (1999).
- <sup>26</sup>J. A. Fernandez-Baca, M. E. Hagen, Pengcheng Dai, F. Ye, J. Kulda, Y. Tomioka, and Y. Tokura, *Physica B* **385–386**, 66 (2006).
- <sup>27</sup>J. W. Lynn, C. P. Adams, Y. M. Mukovskii, A. A. Arsenov, and D. A. Shulyatev, *J. Appl. Phys.* **89**, 6846 (2001).
- <sup>28</sup>D. N. Argyriou, J. W. Lynn, R. Osborn, B. Campbell, J. F. Mitchell, U. Ruett, H. N. Bordallo, A. Wildes, and C. D. Ling, *Phys. Rev. Lett.* **89**, 036401 (2002).
- <sup>29</sup>F. Moussa, M. Hennion, J. Rodríguez-Carvajal, H. Moudden, L. Pinsard, and A. Revcolevschi, *Phys. Rev. B* **54**, 15149 (1996).
- <sup>30</sup>M. Hennion, F. Moussa, J. Rodríguez-Carvajal, L. Pinsard, and A. Revcolevschi, *Phys. Rev. B* **56**, R497 (1997).
- <sup>31</sup>M. Hennion, F. Moussa, G. Biotteau, J. Rodríguez-Carvajal, L. Pinsard, and A. Revcolevschi, *Phys. Rev. Lett.* **81**, 1957 (1998).
- <sup>32</sup>F. Moussa, M. Hennion, G. Biotteau, J. Rodríguez-Carvajal, L. Pinsard, and A. Revcolevschi, *Phys. Rev. B* **60**, 12299 (1999).
- <sup>33</sup>G. Biotteau, M. Hennion, F. Moussa, J. Rodríguez-Carvajal, L. Pinsard, A. Revcolevschi, Y. M. Mukovskii, and D. Shulyatev, *Phys. Rev. B* **64**, 104421 (2001).
- <sup>34</sup>P. Kober-Lehouelleur, F. Moussa, M. Hennion, A. Ivanov, L. Pinsard-Gaudart, and A. Revcolevschi, *Phys. Rev. B* **70**, 144409 (2004).
- <sup>35</sup>M. Hennion, F. Moussa, P. Lehouelleur, F. Wang, A. Ivanov, Y. M. Mukovskii, and D. Shulyatev, *Phys. Rev. Lett.* **94**, 057006 (2005).
- <sup>36</sup>M. Hennion, F. Moussa, G. Biotteau, J. Rodríguez-Carvajal, L. Pinsard, and A. Revcolevschi, *Phys. Rev. B* **61**, 9513 (2000).
- <sup>37</sup>F. Moussa, M. Hennion, F. Wang, P. Kober, J. Rodríguez-Carvajal, P. Reutler, L. Pinsard, and A. Revcolevski, *Phys. Rev. B* **67**, 214430 (2003).
- <sup>38</sup>F. Moussa and M. Hennion, in *Colossal Magnetoresistive Manganites*, edited by T. Chatterji (Kluwer, Dordrecht, 2004).
- <sup>39</sup>M. Hennion and F. Moussa, *New J. Phys.* **7**, 84 (2005).
- <sup>40</sup>M. Hennion, F. Moussa, P. Lehouelleur, P. Reutler, and A. Revcolevschi, *Phys. Rev. B* **73**, 104453 (2006).
- <sup>41</sup>In the academic case of a spin-wave dispersion curve derived from a Heisenberg model, the stiffness constant  $D$  and the exchange couplings  $J_{ij}$  are related:  $D=2Sa^2(J_1+4J_4)$ .
- <sup>42</sup>K. Hirota, N. Kaneko, A. Nishizawa, Y. Endoh, M. C. Martin, and G. Shirane, *Physica B* **237–238**, 36 (1997).
- <sup>43</sup>L. F. Feiner and A. M. Oleś, *Physica B* **259–261**, 796 (1999).
- <sup>44</sup>A. M. Oleś and L. F. Feiner, *Phys. Rev. B* **65**, 052414 (2002).
- <sup>45</sup>Y. Moritomo, T. Akimoto, A. Nakamura, K. Ohoyama, and M. Ohashi, *Phys. Rev. B* **58**, 5544 (1998).
- <sup>46</sup>L. Vasiliu-Doloc, J. W. Lynn, A. H. Moudden, A. M. de Leon-Guevara, and A. Revcolevschi, *Phys. Rev. B* **58**, 14913 (1998).
- <sup>47</sup>L. Vasiliu-Doloc, J. W. Lynn, Y. M. Mukovskii, A. A. Arsenov, and D. Shulyatev, *J. Appl. Phys.* **83**, 7342 (1998).
- <sup>48</sup>Michael C. Martin, G. Shirane, Y. Endoh, K. Hirota, Y. Moritomo, and Y. Tokura, *Phys. Rev. B* **53**, 14285 (1996).